Design and Validation of Ultra Low Thrust Transfers to the Sun-Earth Saddle Point with Application to LISA PathFinder Mission Extension

By Francesco Topputo,[1] Diogene Alessandro Dei tos,[1] Mirco Rasotto[2], and Florian Renk[3]

[1]*Politecnico di Milano, Department of Aerospace Science and Technology, Milan, Italy*
[2]*Dinamica Srl, Milan, Italy*
[3]*European Space Operation Center (ESOC), Darmstadt, Germany*

In this paper we present methods and concepts to design and validate highly nonlinear orbits characterized by ultra low control. These features are met when flying through the Saddle Points, which are location in the Solar System when gravitational accelerations balance. Trajectory optimization is embedded into high-fidelity environments, where accurate description of the spacecraft natural and controlled motion is achieved. Orbit determination and navigation analysis rely on high-fidelity models for both the space and ground segments assets as well. Tools have been developed and applied to the case of the possible mission extension of Lisa Pathfinder.

1. Introduction

Flying in highly nonlinear gravity fields is appealing due to the unique features that can be achieved if these models are properly exploited. Lagrange point orbits, ballistic capture orbits, low-energy transfers, invariant manifolds, etc., are just mere examples of what can be done by using the natural motion of a spacecraft subject to two (or more) gravitational attractions that are comparable. Beside generating orbits that cannot be designed in the classic two-body problem, multi-body models may enable considerable propellant savings, launch window widening, and overall safety increase[1].

More recently, attention has been paid to the exploration of the Saddle Points (SP) in the Solar System[2]. These are locations in the configuration space where the net gravitational acceleration balances. These regions present clean, close-to-zero background acceleration environments where possible deviations from the General Relativity (i.e., the MOND/TeVeS theory) can be tested and quantified[3]. Within the set of SP in the Solar System, the Sun–Earth SP is particularly appealing due to its relatively easy accessibility[4]. Although they are remarkable locations in the Solar System, SP are still unexplored. Their location and the non-equilibrium nature suggest that flying across the SP can be done by exploiting the highly nonlinear, limited control authority orbits described above.

The orbits flying through the SP feature a number of peculiarities, namely, 1) they are highly sensitive to small variations in the initial conditions, 2) a very limited control authority can be exerted*, and 3) the SP has to be targeted with high precision. These demanding requirements make it natural to question about the feasibility of flying through the SP with such underactuated systems in highly unstable vector fields.

In this work, we have formulated methodologies and developed tools to design highly-nonlinear, control-limited orbits flying through the SP, and to assess their feasibility, with a special focus on their navigability. The trajectory design is carried out in a restricted *n*-body problem where the solar radiation pressure as well as the oblateness of the celestial bodies are modeled. Maneuvers are considered impulsive in the first stage of design; they are transformed into continuous, finite-burn arcs in later stages. The feasibility assessment involves developing high-fidelity models for both the space and ground segments assets. An orbit determination algorithm accounts for uncertainties and noise in the spacecraft state, dynamical model, and maneuver execution. The cost to navigate the orbits is also extracted a posteriori by considering the deviations from the nominal solution given by the orbit determination.

The application case is Lisa Pathfinder (LPF). LPF has been flying about Sun–Earth L1 into a Lissajous orbit. Its Drag Free and Attitude Control System (DFACS) is made of three clusters of cold-gas (Nitrogen) thrusters. LPF is also equipped with a gravity gradiometer consisting of two freely floating test masses, separated by a baseline of just under 40 cm. This is an ideal apparatus that can be used to test MOND/TeVeS theories.

2. Transfer Design

The equations of motion for a massless spacecraft are written in a high-fidelity *n*-body problem within a Sun–Earth synodic frame. The model is referred to as roto-pulsating restricted *n*-body problem[5] (RPRnBP). Precise positions and velocities of celestial bodies are retrieved with the SPICE toolkit† as a function of ephemeris epoch, that is TDB seconds after J2000 date (January 1 2000 00^{hr}:00^{min}:00^{sec}). On top of that, the gravity field is perturbed by the action of 1) Solar Radiation Pressure (SRP) acting on the Sun–S/C line and handled with a spherical model, and 2) the planets oblateness, which is embedded as an expansion series in the potential, as function of J_2 and J_n. The equations of motion are

---

* This is because ultra low thrust propulsion (e.g., cold gas thrusters) is preferred to conventional high-thrust propulsion to enable a fine trajectory control and to avoid disturbances due to propellant sloshing.

$$n^2 kC\boldsymbol{\rho}'' + 2n(kC + k\dot{C})\boldsymbol{\rho}' + (\ddot{k}C + 2\dot{k}\dot{C} + k\ddot{C})\boldsymbol{\rho} + \ddot{\boldsymbol{b}} + \sum_{j\in\mathcal{S}}\left[\mu_j \frac{C\boldsymbol{\rho}_j}{k^2\rho_j^3} + \frac{3}{2}\sum_{j\in\mathcal{S}}\mu_j J_{2_j} R_{pl_j}^2\left(\frac{1}{k^4\rho_j^5} + \frac{2I_k}{k^4\rho_j^5} - \frac{5}{k^6\rho_j^7}\right)C\boldsymbol{\rho}_j\right] = \frac{F_0}{m}\frac{C\boldsymbol{\rho}_1}{k^2\rho_1^3}, \quad (1)$$

where $\boldsymbol{\rho}$ and m are the S/C nondimensional position vector in the roto-pulsating frame and its mass, respectively, n is the mean motion of the Earth about the Sun, k their present distance, and $\boldsymbol{b}$ their barycenter; C is the rotation matrix from inertial to RPRnBP, $\mathcal{S}$ the set of celestial bodies influencing the S/C dynamics, μ_j the gravitational parameter of the j-th body, $\boldsymbol{\rho}_j$ its position vector, J_{2_j} its second zonal harmonics coefficient, and R_{pl_j} its mean equatorial radius; F_0 is the force magnitude exerted on the spacecraft due solar pressure, and I_k a three-by-three matrix of zeros except for the third diagonal component, $I_k(3,3) = 1$. Primes indicate indicate derivative with respect to nondimensional time, where dots derivative with respect to dimensioned time[‡]. Eq. (1) is the equation used in the present work for the trajectory design.

The trajectory design workflow consists of 4 phases:

I) In the *exploration* phase, feasible initial solutions are sought by means of a global grid search. Starting from the unstable manifold of L_1 and L_2 halo orbits, ballistic approaches to the SP are classified[§]. The direct numerical simulation parameters are a) the halo orbit amplitude, b) the S/C initial phase along the halo, and c) the initial true date. The search provides sufficient degrees of freedom to achieve numerous ballistic SP close passages (with a grid of $96,000$ points, roughly 1% of the trajectories came to within $10,000$ km of the SP).

II) The *optimization* phase is the core of the transfer design. A direct transcription of the dynamics, coupled with a multiple shooting method, is used to tune a series of impulsive maneuvers to precisely target the SP.

III) The *finite burn* phase is required to translate the optimal impulsive maneuvers into a series of finite thrust arcs, compatibly with the engine ultra-low control capabilities.

IV) For augmented accuracy, the thrusting direction of the output solutions is further refined in an Earth-centered inertial frame. This the *refinement* phase.

2.1. Multiple burns multiple shooting

The SP passage is targeted by means of a multiple shooting technique that embeds a series of impulsive burns instantaneously modifying the S/C velocity. This is a general state-to-position optimal transfer where the initial time is an optimization parameter and the final conditions depend on the actual SP position, which is a function of time. The number of maneuvers, *NoM*, is prescribed. Referring to Fig. 1 we define:

---

‡ Mixed derivative notation in Eq. (1) acknowledges that ephemeris data is numeric, discrete, and provided for dimensional time.

§ The SP is located at a distance of approximately 258,800 km from the Earth, along the Sun–Earth line, between the Sun and the Earth.

- *Segment* as the part of the trajectory that stems from the multiple shooting transcription;

- *Arc* as the ballistic stretch separated by maneuvers;

- *Leg* as the whole S/C trajectory between SP passages.

In this analysis, there are $m - 1$ segments per arc (m is the number of discrete points for the multiple shooting time discretization), $NoM + 1$ arcs per leg, and as many legs as the number of consecutive SP passages. For numerical purposes, each arc can be considered as a separate two-point boundary value problem (TPBVP), where boundary conditions on both temporal extrema depend either on 1) the initial conditions and the state of the following adjoint arc, 2) the states of two adjoint arcs, or 3) the state of the previous adjoint arc and the final conditions. In this way the optimization can be carried out by patching together several multiple shooting arcs. The patching condition requires continuity in position and a fixed jump in velocity that represents the impulsive maneuver. The multiple shooting procedure is briefly recalled here for convenience. It is applied to a general arc j of the trajectory, and superscripts in the variables indicate the arc to which they belong. The proper selection of variables and an ad-hoc transcription strategy have significant impact on the algorithm efficiency and performance[6].

A TPBVP[7] consists of finding $\boldsymbol{x}(t)$, $t \in [t_0, t_f]$, such that

$$\dot{\boldsymbol{x}} = \boldsymbol{f}(\boldsymbol{x}, t), \qquad \boldsymbol{h}(\boldsymbol{x}(t_0), \boldsymbol{x}(t_f)) = \boldsymbol{0}. \qquad (2)$$

In this context, the dynamics in (2) is the state space representation of Eq. (1) ($\boldsymbol{x}$ is 6-dimensional). The function $\boldsymbol{h}$ specifies nonlinear boundary conditions, needed to well-pose the problem[8]. Problem (2) is solved for a finite set of variables[9].

The solution is discretized over m points $t_0^{(j)} = t_1^{(j)} < t_2^{(j)} < \cdots < t_m^{(j)} = t_f^{(j)}$; that is, $\boldsymbol{s}_k^{(j)} = \boldsymbol{x}(t_k^{(j)})$, $k = 1, \ldots, m$. This defines $m - 1$ segments in which a TPBVP is solved by enforcing continuity at both ends. This shortens the duration of the original solution and reduces sensitivity. Let the defect vector be

$$\boldsymbol{\zeta}_k^{(j)} = \boldsymbol{\varphi}(\boldsymbol{s}_k^{(j)}, t_k^{(j)}; t_{k+1}^{(j)}) - \boldsymbol{s}_{k+1}^{(j)}, \quad k = 1, \ldots, m-1, \qquad (3)$$

where $\boldsymbol{\varphi}(\boldsymbol{x}_0, t_0; t)$ is the flow (i. e., solution) at time t of Eq. (2) starting from initial conditions $(\boldsymbol{x}_0, t_0)$. A schematic representation of the defect vectors and the ballistic arcs is shown in Fig. 1. The problem is to determine the states $\boldsymbol{s}_k^{(j)}$ such that

$$\boldsymbol{\zeta}_k^{(j)} = \boldsymbol{0}, \quad k = 1, \ldots, m-1, \quad \text{and} \quad \boldsymbol{h}^{(j)}(\boldsymbol{s}_1^{(j)}, \boldsymbol{s}_m^{(j)}) = \boldsymbol{0}. \quad (4)$$

In Eqs. (4) there are $6m$ unknowns (the states $\boldsymbol{s}_k^{(j)}$) and $6m$ equations (6 boundary conditions and $6(m - 1)$ defect constraints). This is the classic multiple shooting method. Within this framework, patching together adjoint arcs simply translates in the proper mathematical definition of the function $\boldsymbol{h}^{(j)}$, expressing
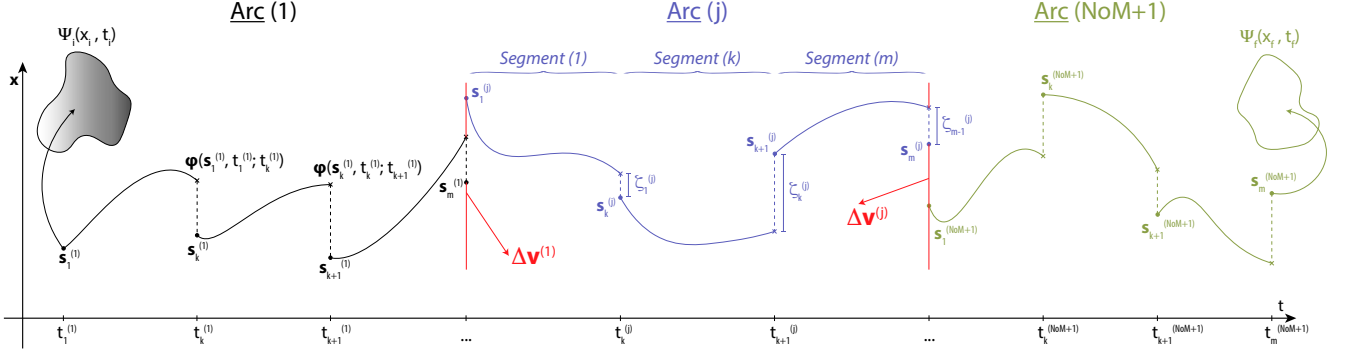
Fig. 1.: Multiple shooting strategy.

the boundary conditions between those:

$$h^{(j)} : \begin{cases} s_1^{(1)} = x_0; \\ s_1^{(j)} - s_m^{(j-1)} = \delta_v \Delta v^{(j-1)}, & j = 1, \dots, NoM; \\ s_m^{(NoM+1)} = x_f; \end{cases} \quad (5)$$

where $\delta_v = [0_3, I_3]^T \in \mathbb{R}^{6 \times 3}$ is an operator that maps velocity in its correct position. Note that both x_0 and x_f can be function of time. This is important because the initial/final state might be a prescribed trajectory (e. g., LPF).

Variables.   The number of unknowns, N_{var}, of this problem depends on the number of maneuvers and the number of segments of the multiple shooting, namely

$$N_{var} = (6m + 2)(NoM + 1).$$

They represents $m(NoM+1)$ six-dimensional states for the multiple shooting, and 2 times per arc. The nonlinear programming (NLP) variables embed hence the initial and final times, that are allowed to vary. The variables are collected in vector

$$y = (s_1^{(1)}, \ s_m^{(1)}, \ s_k^{(j)}, \ s_m^{(NoM+1)}, \ t_1^{(1)}, \ t_m^{(1)}, \ t_1^{(j)}, t_m^{(NoM+1)}), \quad (6)$$

where it is noted that variables are repeated at arc interfaces. This reduces the mutual dependence among arcs, leading to more sparse Jacobian, better behaved coupling only due to continuity conditions, with the drawback of tracking a higher number of unknowns.

Objective function.   A relevant space mission parameter is the Δv consumption, which is intimately related to on-board propellant mass. Accordingly, the objective function is,

$$J(y) = \sum_{j=1}^{NoM} \|\Delta v^{(j)}\|^2. \quad (7)$$

Constraints.   These are subdivided into:

- Equality constraints
  - (i) Time and position continuity at arcs interfaces,
  - (ii) Defect vectors must be null to ensure continuity between adjoint segments,
  - (iii) Boundary conditions enforcement.

- Inequality constraints

- (i) The maximum time for reaching the SP is bounded to 5 years, and each arc should last minimum 2 days,

- (ii) The nature of the problem suggests that several solutions exist corresponding to a wide range of control authority. Here, control budget is limited to 20 m/s.

- (iii) For feasible impulsive-to-finite maneuver conversion, it is necessary to allow enough post-maneuver time. This is done by estimating the thrusting time as a function of the Δv, and engine performances.

There are a total of $4NoM + 6(m - 1)(NoM + 1) + 9$ equality constraints, $c_{eq} = 0$, and $2NoM+3$ inequality constraints, $c \le 0$:

$$c_{eq} = \begin{pmatrix} r_m^{(j)} - r_1^{(j+1)} \\ t_m^{(j)} - t_1^{(j+1)} \\ \zeta_k^{(j)} \\ s_1^{(1)} - x_0 \\ \delta_r s_m^{(NoM+1)} - r_{SP}(t_m^{(NoM+1)}) \end{pmatrix}, \quad (8)$$

$$c = \begin{pmatrix} t_1^{(j)} - t_m^{(j)} + 2 \text{ days} \\ t_m^{(NoM+1)} - 5 \text{ years} \\ \sum_{j=1}^{NoM} \|\Delta v^{(j)}\| - 10 \text{ m/s} \\ \frac{m_{S/C} \|\Delta v^{(j-1)}\|}{T_{max}} - (t_m^{(j)} - t_1^{(j)}) \end{pmatrix}. \quad (9)$$

In the last component of Eq. (8), $\delta_r = [I_3, 0_3] \in \mathbb{R}^{3 \times 6}$ is an operator that maps state to position. (Γ_{SP} is referred to the SP miss distance.) Regarding the last of Eq. (9), numerical simulations have shown that this is always an overestimation of the time necessary to spread the maneuver.

Problem 1. The problem of precisely hitting the SP by resorting to a series of impulsive maneuvers can be stated as:

$$\min_{y} J(y) \quad s.t. \quad \begin{cases} c_{eq} & = 0, \\ c & \le 0. \end{cases} \quad (10)$$

The Matlab *active-set* algorithm has been used to solve the NLP.

Fig. 2 shows and example of trajectory to the SP. The light-colored line is the guess solution of the exploration phase, whereas the dark line represents the actual trajectory. A series of 6 impulsive maneuvers place the spacecraft in a SP-bound path. Relevant parameters of the trajectory are found in Table 1.
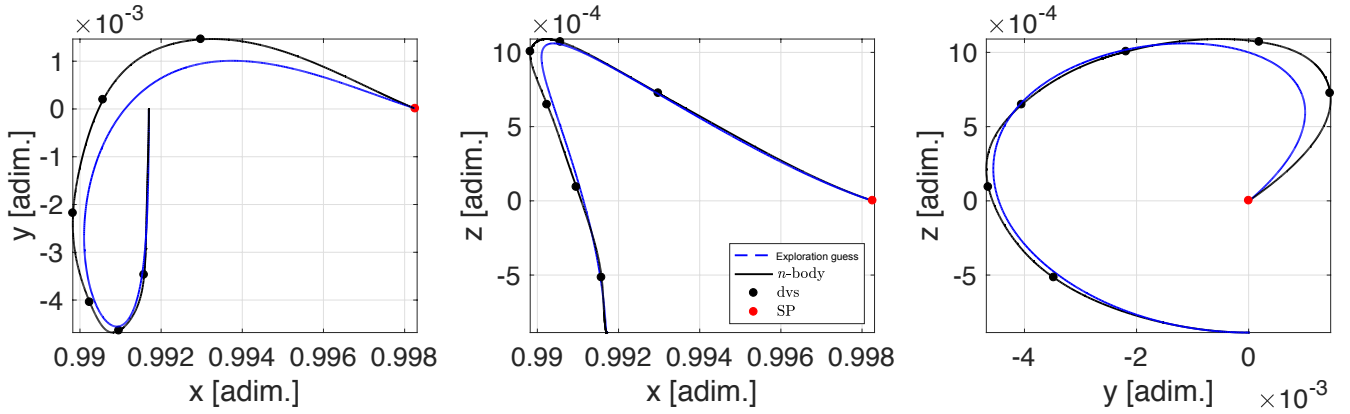
Fig. 2.: Example of trajectory to the SP.

Table 1.: Parameters for the direct SP transfer orbit refinement.

NoM	Δv	TOF	t_{SP}	$\|\Gamma_{SP}\|$
[m]	[m/s]	[days]	[TDB]	[m]
6	16.23	122.5	07/18/17, 17:02:56	$0.14e-3$

3. Finite burn maneuvers

An exact impulsive to finite burn maneuver conversion is one that produces a finite burn solution whose final state is equal to the final position and velocity of the original post impulse trajectory at the time the finite burn maneuver ends. This means that the ballistic (un-thrusted) phases of the finite burn trajectory are identical to the ballistic phases of the impulsive trajectory. The single impulsive maneuver may be part of a more complex multi-impulse trajectory. An approach to this problem is to convert each impulsive maneuver separately[¶]. It is assumed that the end time of a finite burn maneuver will be less than or equal to the start time of the next finite burn maneuver that is used to replace the next impulsive maneuver, if it exists. The latter is compliant with the the nonlinear constraint of Section **2.1.**.

The minimum finite burn time optimization problem for a single impulse, as defined here, is treated as a pseudo-rendezvous problem where the target particle flies along the post-impulse trajectory[10]. Referring to Fig. 3, the chase particle is the spacecraft itself that flies along the pre-impulse trajectory and is required to rendezvous with the target particle. In this figure, the time of the impulse is t_i, and the state of the particle on the finite burn trajectory is also identified at the same epoch.

The information available from the impulsive maneuver is used to estimate the start/end times of the time optimal finite burn, along with the values of the locally referenced spherical angles and their first and second time derivatives. Azimuth and elevation time profiles for the thrust are approximated as quadratic polynomials of time with unknown coefficients, leading to a sub-optimal solution. A direct method with explicit numerical integration is used to optimize this finite burn model solution.

The impulsive to finite burn conversion is done assuming ideal engine with constant maximum thrust and exhaust velocity.
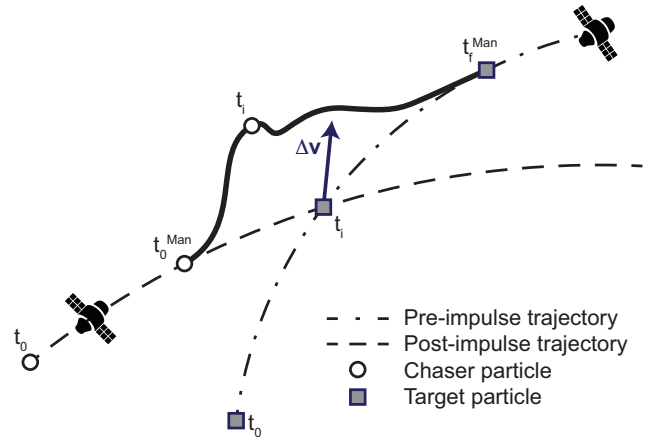

[¶] The conversion of a multi-impulse trajectory to an equivalent multi-finite burn trajectory is a separate problem, with many more issues, and is also not considered in this study.
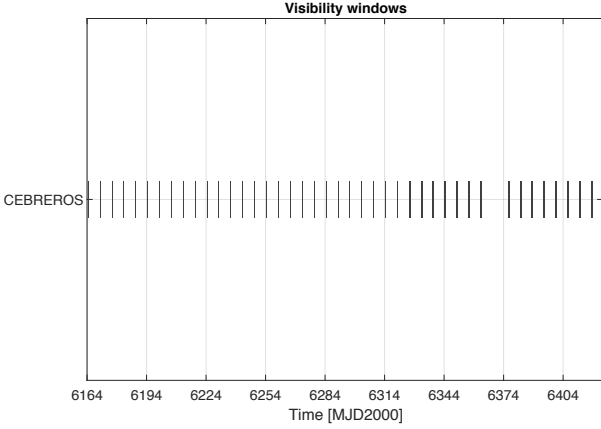

Fig. 3.: Impulsive to finite burn maneuver pseudo-rendezvous.

4. Navigation Analysis

To assess the feasibility of flying preliminary designed orbits, a navigation tool has been implemented. This includes the development of high-fidelity models for both space and ground segments assets, as well as an orbit determination algorithm which uses simulated measurements to reconstruct the spacecraft state.

4.1. Tracking windows

The identification of tracking/coverage windows for all the selected ground stations represents the first step of the navigation analysis, required to generate the radiometric data and ultimately simulate the estimation process.

More in details, a coverage window from one ground station is defined as an un-thrusted portion of the trasfer trajectory without solar conjunction[11] or Moon occultations and in which the corresponding elevation and linking constraints are satisfied.

After their identification, resulting visibility windows may also be filtered with respect to other criteria such as:

- *overlaps*, whenever the spacecraft is in view of multiple ground stations, to avoid simultaneous radiometric data;

- *short durations*, to ensure a minimum duration, required for instrument calibrations process;

- *long durations*, to limit the time interval available for nav-

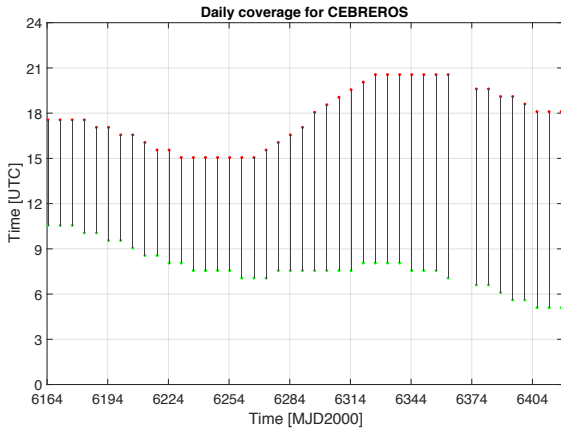Fig. 4.: Coverage windows from Cebreros ground station.

Fig. 5.: Daily coverage duration from Cebreros ground station.

igation purpose;

- *windows frequency*, to avoid dealing with coverage windows very close in time, which may not reflect real life conditions and typically do not lead to significant improvements in the orbit knowledge[12].

The coverage windows obtained from Cebreros ground station for the presented transfer are shown in Fig. 4. Note that these have already been filtered assuming a minimum separation interval of 5 days between two consecutive windows. The daily coverage evolution along the transfer is reported in Fig. 5.

4.2. Measurements generation

Radiometric data including two-way Doppler and range measurements are generated from selected ground stations. Their accuracy is affected by several errors such as Earth orientation, clock instabilities, delays of the signal due to both instruments (thermal noise), and transmission media. All these sources are reduced to a set of random and bias errors on the simulated measurements, whose values are specified in Table 2.

An example of the radiometric data simulated for the LPF case is reported in Figs. 6 and 7, where range and range-rate measurements from Cebreros ground stration are shown.

4.3. Covariance analysis

The main goal of this section is to determine the achievable level of accuracy in spacecraft position and velocity knowledge.

Table 2.: Range and Doppler measurements assumptions.

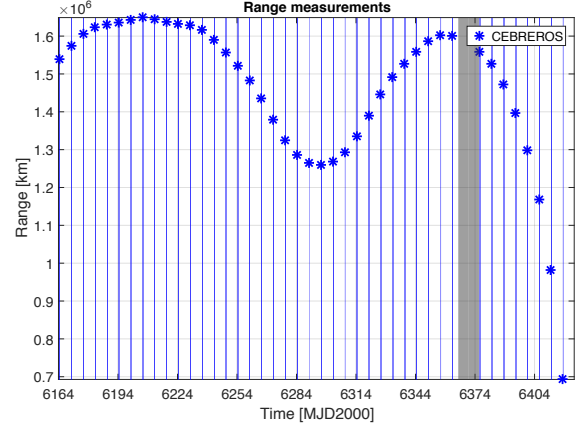| Parameter	Value
Range frequency	once per pass
Range noise (1σ)	20 m
Range bias	20 m
Doppler frequency	once every 10 min
Doppler noise (1σ)	0.03 mm/s
Doppler bias	0 mm/s

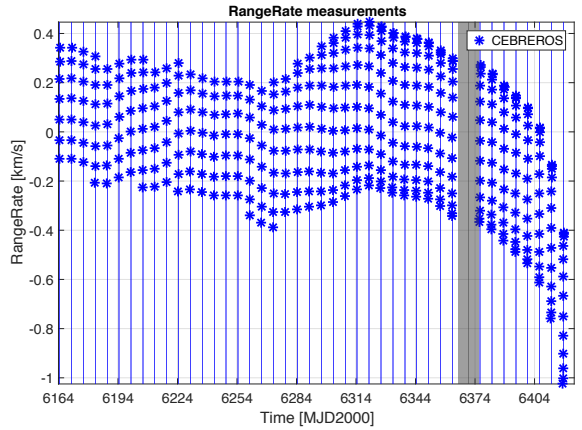
Fig. 6.: Range measurements (Cebreros ground station).

Fig. 7.: Range-rate measurements (Cebreros ground station).

A Square Root Information Filter (SRIF), as presented in Ref. 13), is used to perform the orbit determination (OD) process and derive the state estimates. The initial uncertainty is assumed to be 100 km in each component of position, 1 m/s in each component of velocity and 0.1 kg in mass. Starting from the a priori information, the SRIF algorithm is run with a mapping time of 0.25 days. At each measurement epoch, radiometric data are processed to obtain the knowledge update in terms of information array. In case no measurements are available, state and covariance matrix are simply propagated forward, up to the next mapping time. Proceeding in this way, the state estimates are sequentially updated, leading to the final position and velocity knowledge profiles. By fixing a certain threshold, a parametric analysis can also be performed to determine the minimum tracking frequency required to guarantee the desired accuracy level. Note that the adopted filter implementation allows accounting for several error sources:
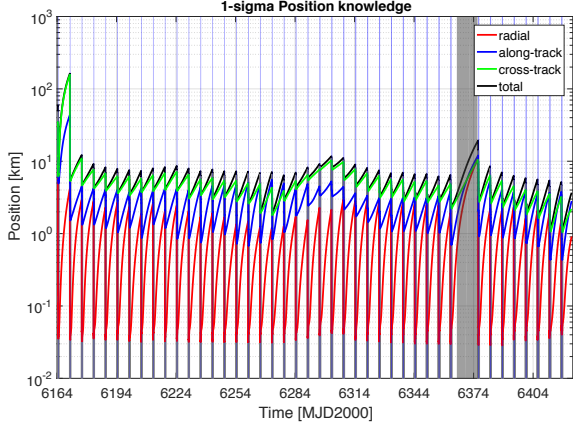
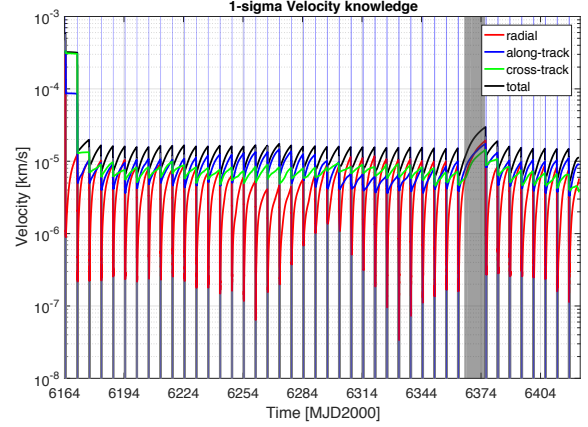Fig. 8.: 1σ achievable knowledge in spacecraft position.

Fig. 9.: 1σ achievable knowledge in spacecraft velocity.

- the effects of systematic/bias errors, through a consider co-variance approach[13]. Belong to this class, errors such as:

  1. ground station location biases: assumed equal to 30 cm in equatorial plane error and 1 m out of equatorial plane error.

  2. systematic errors in the measurement modelling (e.g due to system calibration errors), see Table 2.

- the effects of exponentially correlated random variables (ECRV), such as:

  1. Stocastic components of the solar radiation pressure, modeled as an ECRV with a magnitude of 10% of the nominal force and a correlation time of 1 day.

  2. Thrust variables (magnitude and direction) assumed as ECRV with a 1σ error of 1% in modulus and 0.5° in pointing angle, correlation time of 1 day.

  3. Residual accelerations, modeled as an ECRV with a steady state uncertainty of 3 cm/s/day (3.5×10^{-10} km/s^2, 3σ).

The inclusion of all these effects is mainly aimed at compensating for differences between physical models and real world, and therefore at assessing the feasibility of flying such orbits in a real environment.

Results are given in Figs. 8 and 9, where the position and velocity knowledge for the proposed transfer solution are reported. Clearly, the achievable accuracy in the state knowledge at the very beginning is quite poor and mainly depends on the a priori covariance matrix. As soon as the number of processed measurements increases, the accuracy level improves, although a change in the knowledge can be seen almost in the middle of the transfer. This is due to a low level of spacecraft observability which occurs when the spacecraft is crossing the equator plane. An increment in the knowledge uncertainty is also observable in the low-thrust arc (grey shaded area in the plot), where the combination of zero tracking data with the magnitude and pointing noises, deteriorates the achievable accuracy.

4.4. Navigation costs

To estimate the navigation costs the following approach is assumed:

i. The solution is partitioned into small arcs. Let t_j and t_{j+1} be the initial and final time associated to the j-th arc, respectively, and let $\Delta t_j = t_{j+1} - t_j$ be its duration.

ii. At time t_j, the spacecraft position and velocities are off from the nominal solution by $\delta \boldsymbol{r}_j$ and $\delta \boldsymbol{v}_j$, respectively. These deviations are computed starting from the 1σ, 2σ and 3σ error ellipsoids. The probability of the state estimate error falling inside these ellipsoids, assuming a trivariate Gaussian density function, is 0.200, 0.739, and 0.971, respectively[13].

iii. A navigation maneuver $\Delta \boldsymbol{v}_j$ at time t_j has to be accounted to correct the deviated state and minimize its distance from the nominal solution at time t_{j+1}. The magnitude of this maneuver is computed as shown in Ref. 14):

$$\Delta \boldsymbol{v}_j = k \left(\delta \boldsymbol{v}_j + \frac{\delta \boldsymbol{r}_j}{\Delta t_j} \right) + \boldsymbol{a}_{\text{err}} \Delta t_j, \qquad (11)$$

where k is a systematic propagation error equal to 1.1 and $\boldsymbol{a}_{\text{err}}$ is an external error applied periodically of 10^{-11} km/s^2.

iv. The logic in i–ii above is repeated for the whole duration of the transfer (from t_0 to t_f). In this way a correction cycle of periodicity Δt_j is obtained to limit the growth of the perturbing trajectory. The cost of this correction cycle is $\Delta v_{\text{nav}} = \sum_j \Delta v_j$.

The navigation cost for a Δt_j of 5 days is reported in Fig. 10. As expected, the required Δv_j becomes larger whenever the state knowledge accuracy decreases. The final Δv_{nav} values needed to navigate the presented solution are 2.387 m/s (1σ), 4.766 m/s (2σ) and 7.168 m/s (3σ).

To ensure the feasibility of the maneuver Δv_j within the time interval Δt_j, the navigation correction duration is computed considering the current spacecraft mass as well as the maximum thrust available. As can be seen from the results depicted in Fig. 11, the needed time is always below the value of 5 days assumed for the correction cycle.

By varying the value of Δt_j it might be possible to determine the optimal navigation interval; that is, the frequency of the correction cycle that yields the least navigation cost, while still respecting the mission requirements. Figure 12 illustrates how this value changes with the value of Δt_j, and therefore with the
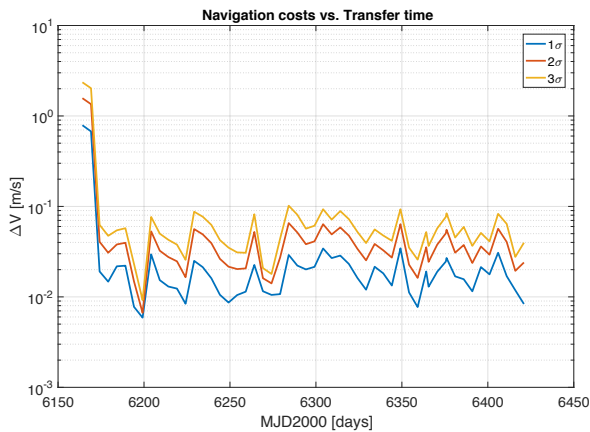
Fig. 10.: Navigation costs (correction cycle: 5 days).
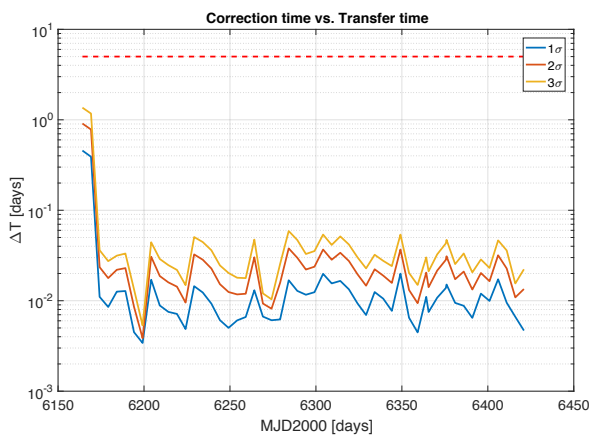

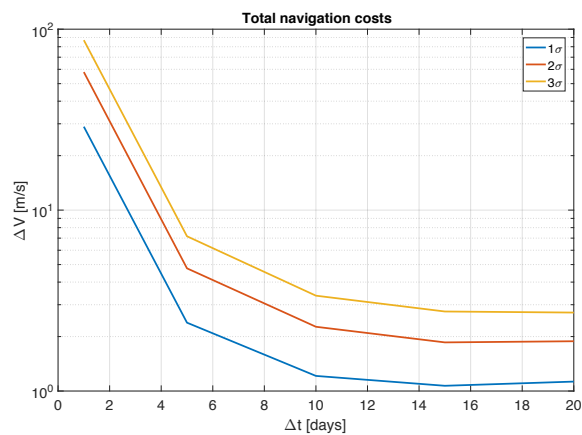Fig. 11.: Navigation correction duration (corr. cycle: 5 days).

Fig. 12.: Navigation cost vs frequency of the correction cycle.

frequency of the correction cycle. As expected a higher Δv_{nav} is found for short time intervals, whereas an asymptotic behaviour is reached for larger Δt_j.

These costs are added to the Δv_{nom}, output of the design phase, to get an overall Δv budget to fly the ultra low thrust orbits.

5.   Conclusion

In this paper we have summarized the heritage accumulated in designing and validating ultra low thrust transfers to the SP.

These are peculiar orbits that require sophisticated methods for design and navigation analysis. The method and tools developed have been applied to the possible mission extension of LPF, though they can be used to treat generic opportunity missions from the Lagrange point orbits as well as dedicated missions to the SP.

Acknowledgments

References

1) Topputo, F., and Belbruno, E.: Earth–Mars Transfers with Ballistic Capture, *Celestial Mechanics and Dynamical Astronomy*, **121** (2015), pp. 329–346.

2) Trenkel, C., Kemble, S., Bevis, N., and Magueijo, J.: Testing Modified Newtonian Dynamics with LISA Pathfinder, *Advances in Space Research*, **50** (2012), pp. 1570–1580.

3) Fabacher, E., Kemble, S., Trenkel, C., and Dunbar, N.: Multiple Sun–Earth Saddle Point flybys for LISA Pathfinder, *Advances in Space Research*, **52** (2013), pp. 105–116.

4) Cox, A., and K. Howell, Transfers to a Sun–Earth Saddle Point: An Extended Mission Design Option for LISA Pathfinder, 26th AAS/AIAA Space Flight Mechanics Meeting, Napa, USA, Paper AAS 16-299, 2016.

5) Dei Tos, D.A., and Topputo, F.: Trajectory refinement of three-body orbits in the real solar system model. *Advances in Space Research*. **59** (2017), pp. 2117–2132.

6) Stoer, J., and Bulirsch, R.: Introduction to numerical analysis. Springer, 2012.

7) Armellin, R., and Topputo, F.: A Sixth-Order Accurate Scheme for Solving Two-Point Boundary Value Problems in Astrodynamics, *Celestial Mechanics and Dynamical Astronomy*, **96** (2006), pp. 289–309.

8) Bolle, A., and Circi, C.: A Hybrid, Self-Adjusting Search Algorithm for optimal space trajectory design, *Advances in Space Research*, **50** (2012), pp. 471–488.

9) Mingotti, G., Topputo, F., and Bernelli-Zazzera, F.: Transfers to Distant Periodic Orbits around the Moon via their Invariant Manifolds, *Acta Astronautica*, **79** (2012), pp. 20–32.

10) Ocampo, C., and Munoz, J.-P.: Variational equations for a generalized spacecraft trajectory model, *Journal of guidance, control, and dynamics*, **33** (2010), pp. 1615–1622.

11) Yarnoz, D., Jehn, R., and Croon, M.: Interplanetary navigation along the low-thrust trajectory of BepiColombo, *Acta Astronautica*, **59** (2006), pp. 284–293.

12) Virtanen, J.: Asteroid orbit computation, *Asteroids III*, University of Arizona Press, (2002), pp. 27.

13) Schutz, B., Tapley, B., and Born, G.H.: Statistical Orbit Determination, Academic Press, 2004.

14) Toullec B.: New trajectories to test MOND/TEVES with Lisa Pathfinder, 61st International Astronautical Congress, Prague, Czech Republic, Paper IAC-10.E2.1.6, 2010.